

This is a repository copy of *Hysteresis features of the transition-metal dichalcogenides VX₂ (X = S, Se, and Te).*

White Rose Research Online URL for this paper:

<https://eprints.whiterose.ac.uk/id/eprint/163982/>

Version: Accepted Version

Article:

Vatansever, E., Sarikurt, S. and Evans, R. F.L. orcid.org/0000-0002-2378-8203 (2018)
Hysteresis features of the transition-metal dichalcogenides VX₂ (X = S, Se, and Te).
Materials Research Express. 046108. ISSN: 2053-1591

<https://doi.org/10.1088/2053-1591/aabca6>

Reuse

Items deposited in White Rose Research Online are protected by copyright, with all rights reserved unless indicated otherwise. They may be downloaded and/or printed for private study, or other acts as permitted by national copyright laws. The publisher or other rights holders may allow further reproduction and re-use of the full text version. This is indicated by the licence information on the White Rose Research Online record for the item.

Takedown

If you consider content in White Rose Research Online to be in breach of UK law, please notify us by emailing eprints@whiterose.ac.uk including the URL of the record and the reason for the withdrawal request.

E. Vatansever^{1,*}, S. Sarikurt¹, and R.F.L. Evans²

¹*Department of Physics, Dokuz Eylül University, TR-35160, Izmir-Turkey and*

²*Department of Physics, University of York, YO10 5DD, York-United Kingdom*

(Dated: March 20, 2018)

Very recently, it has been shown that vanadium dichalcogenides (VX_2 , $X=S, \text{Se}$ and Te) monolayers show intrinsic ferromagnetism, and their critical temperatures are nearly to or beyond room temperature. Hence, they would have wide potential applications in next-generation nanoelectronic and spintronic devices. In this work, being inspired by a recent study we systematically perform Monte Carlo simulations based on single-site update Metropolis algorithm to investigate the hysteresis features of VX_2 monolayers for a wide range of temperatures up to 600 K. Our simulation results indicate that, both remanence and coercivity values tend to decrease with increasing temperature. Furthermore, it is found that hysteresis curves start to evolve from rectangular at the lower temperature regions to nearly S-shaped with increasing temperature.

PACS numbers: 75.60.Ej, 75.70.Ak, 75.30.Kz, 75.40.Mg

Keywords: Magnetic hysteresis, Monte Carlo simulation, Two-dimensional materials

I. INTRODUCTION

In recent years, two-dimensional (2D) monolayers such as boron nitride (BN) [1], silicene [2], germanene [3], arsenene and antimonene [4], phosphorene [5] and transition metal dichalcogenides (TMDs) [6–8] have attracted considerable attention beyond graphene due to their remarkable structural, electronic, optical and magnetic properties. Among these 2D materials, TMDs have extensive and growing application areas ranging from electronics to energy storage [9–14].

Most of the primitive TMDs are non-magnetic and these materials could gain magnetic properties by applying strain or introducing transition metal atoms, point defects or non-metal element adsorption [15–20]. In recent years, the effect of tensile strain on magnetic moments of monolayered MX_2 ($M=V, Nb$; $X=S, \text{Se}$) structures have been demonstrated by several researchers [21–23]. These studies pointed out that electronic and magnetic properties can be manipulated by applying a biaxial compression or tensile strain. Due to existing intrinsic ferromagnetism and semiconducting properties in VX_2 ($X=S, \text{Se}$ and Te) monolayer structures, **it is not necessary to expose these materials under the effect of tensile strain or to doping of the monolayer structure with either transition metals or non-metallic atoms [24, 25]. So, TMDs such as pristine VX_2 monolayers could be fabricated without either applying strain or introducing transition metal atoms or native defects.**

In the 1970s, bulk VS_2 was synthesized for the first time [26]. A few-layer VS_2 [7, 24, 27–31] has been synthesized in both hexagonal (H- VS_2) and trigonal (T- VS_2) structures while the bulk and few-layer VSe_2 [32–34] and bulk VT_{e2} [35] can only be successfully synthesized in the trigonal structure. As far as we know, the synthe-

sis of monolayer VX_2 ($X=S, \text{Se}$ and Te) has not been experimentally demonstrated to date.

Electronic and magnetic properties of VX_2 monolayers ($X=S, \text{Se}$ and Te) have been investigated in numerous studies using first-principles calculations based on density functional theory (DFT) [21, 23–25, 27, 29, 36–46]. For example, Ma et al. [21] reported that pristine 2D VX_2 ($X=S, \text{Se}$) monolayers exhibit magnetic ordering and that they have two stable magnetic structures, one being ferromagnetic (FM) while the other is antiferromagnetic (AFM). They performed calculations to obtain the magnetic behaviour of the ground state for VX_2 monolayers and found out that the ground states of both structures are FM. This ground state characteristic has been explored in various studies [21, 25, 40, 41, 44].

According to the results of first-principles calculations, it has been previously stated that the total magnetic moment has the main contribution from V atoms while X atoms only give a small contribution to the magnetism of VX_2 ($X=S, \text{Se}$). In the case of VS_2 ; the magnetic moment values have been obtained as $0.486\mu_B$ [21], $0.51\mu_B$ [24], $0.858\mu_B$ [40] on each V atom and $-0.026\mu_B$ [21], $0.03\mu_B$ [24], $0.047\mu_B$ [40] on each S atom. In the VSe_2 and VT_{e2} case, the magnetic values have been reported as $0.680\mu_B$ [21], $0.951\mu_B$ [40] per V atom, $0.048\mu_B$ [21], $0.062\mu_B$ [40] per Se atom, and $0.986\mu_B$ [40] per V atom, $0.096\mu_B$ [40] per Te atom, respectively.

Gao et al. [24] have experimentally demonstrated that ultrathin VS_2 nanosheets with less than five layers represent room temperature FM behavior combined with weak antiferromagnetism. According to the results obtained from the experiment performed at room temperature, the nanosheet displays clear hysteresis in the low applied field whereas it shows paramagnetic behaviour in the high field regime. They also carried out magnetization versus magnetic field (M-H) curve measurement for temperature range from 50K to 300K and for all different temperature values they observed the pro-

*Electronic address: erol.vatansever@deu.edu.tr

nounced S-shaped curve, which is a characteristic of ferromagnetism [47, 48]. They revealed that the saturation magnetization and coercive field decrease with increase of temperature. Furthermore, they verified their experimental results that point out the ferromagnetic ground state by performing total energy calculations.

Kan et al. [23] studied the comparative stability of both H- and T-structures of VS₂ monolayer using DFT with generalized gradient approximation (GGA) functionals. **They conclude** that H-structure has a indirect semiconducting character with a small band gap of 0.187 eV whereas T-structure has a metallic character [21, 27, 29, 49] and H-structure is more stable than the T-structure. They also obtained the semiconductor character of H-structure of VS₂ monolayer using GGA plus on-site Coulomb interaction U (GGA+U, $U = 3$ eV) and Heyd–Scuseria–Ernzerhof (HSE06) hybrid functional. The band gap energies were calculated as $E_{\text{gap}} = 0.721$ eV and $E_{\text{gap}} = 1.128$ eV in respective order. Besides these results, Kan et al. also pointed out that both structures are magnetic and T-structure of VS₂ monolayer has lower magnetism ($0.43\mu_B$ per unit cell) in comparison with H-structure ($1\mu_B$ per unit cell). In a previous study by Zhang et al. [29], for the bulk structures the total magnetic moments of hexagonal and trigonal VS₂ were estimated as $0.85\mu_B$ and $0.31\mu_B$, respectively. Due to the difference between magnetic moment values of T and H-structures, it can be deduced that both monolayer and bulk H-VS₂ structures exhibit greater magnetism than T-structures and so the magnetic moment significantly depends on the crystal structure. More recently, Fuh et al. [25] reported that H-VX₂ monolayer structures have indirect energy band gap with respective small band gap energies of 0.05, 0.22, and 0.20 eV using GGA DFT functionals. They also considered different exchange-correlation functionals such as GGA+U ($U = 2$ eV) and HSE06 hybrid functional to examine the electronic band structure of H-VX₂ monolayers. In addition, they performed GW calculation method to get an accurate value of the semiconducting band gap. The respective energy band gaps were reported as $E_{\text{gap}} = 1.334, 1.2, 0.705$ eV for VS₂, VSe₂ and VTe₂. Furthermore, Huang et al. [43] and Zhuang et al. [44] performed electronic band structure calculations for H-VS₂ monolayer by using GGA+U ($0 \leq U \leq 4$ eV) and Local Density Approximation (LDA)+U ($0 \leq U \leq 5$ eV), respectively and HSE06 functionals. They all found out that H-VX₂ monolayer structures are semiconductors.

On the other hand, Fuh et al. [25] also performed Monte Carlo simulations and obtained the Curie-temperatures as 292, 472, and 553 K for VS₂, VSe₂, and VTe₂ monolayers, respectively. The Curie temperature values obtained using mean field theory are reported by Pan [40] as follows: 309 K for VS₂, 541 K for VSe₂ and 618 K for VTe₂ monolayers. These Curie temperatures reveal that the unique ferromagnetic character can be achieved close to or well beyond the room temperature.

In this paper, we comprehensively investigate

the temperature dependencies of remanence magnetization, coercivity and hysteresis behaviors of monolayer H-VX₂ (X=S, Se, and Te) structures using Monte Carlo simulations with single-site update Metropolis algorithm. The recent theoretical and experimental studies have clearly pointed out the favorable magnetic ground states, magnetic moment values and Curie temperature values of related monolayer structures. We believe that our Monte Carlo simulation results obtained in this work may be beneficial for both experimental and theoretical point of views.

II. MODEL AND SIMULATION DETAILS

We study hysteresis features of the VX₂ (X=S, Se and Te) monolayers on a hexagonal crystal structure under the influence of a magnetic field. The spin Hamiltonian of the considered systems can be written as follows:

$$\begin{aligned} \mathcal{H} = & -J_1 \sum_{\langle ij \rangle} \mathbf{S}_i \cdot \mathbf{S}_j - J_2 \sum_{\langle\langle ij \rangle\rangle} \mathbf{S}_i \cdot \mathbf{S}_j \\ & -k \sum_i (S_{ix}^2 + S_{iy}^2) - g\mu_B H \sum_i S_{ix}. \end{aligned} \quad (1)$$

Here, \mathbf{S}_i and \mathbf{S}_j are the classical Heisenberg spins with unit magnitude at the site i and j in the system. J_1 and J_2 represent nearest neighbour (NN) and next-nearest neighbour (NNN) spin-spin couplings, respectively. $\langle \dots \rangle$ and $\langle\langle \dots \rangle\rangle$ denote the summation over the NN and NNN spin pairs through the system, respectively. k term corresponds to the magnetic anisotropy energy of the system. g, μ_B and H are Landé-g constant, Bohr magneton and magnetic field terms, respectively. The first two summations are over the NN and NNN spin pairs while the last two summations are over all of the lattice points in the system. We follow the Ref. [25] for the real values of the exchange couplings and magnetic anisotropy energy. We note that in Table 2 and 4 of Ref. [25], the authors give the calculated magnetic anisotropy energies and exchange interaction parameters of VS₂, VSe₂ and VTe₂ monolayers, respectively.

We use Monte Carlo simulation with single site update Metropolis algorithm [50, 51] to understand the magnetic properties of the system on a $L \times L$ hexagonal crystal structure. Here, L is the linear size of the hexagonal lattice, and it is fixed as 120 through this work. We select the boundary conditions such that they are periodic in all directions. The simulation process can be briefly summarized as follows. Magnetic hysteresis curves are generated over the 50 independent sample realizations. In each sample realization, the simulation starts at high temperature value using random initial spin configuration. It slowly cooled down until the temperature reaches a specific temperature value in the presence of a magnetic field $H = 1T$ applied in x -direction of the system. Then,

using the obtained last spin configuration as initial configuration, the decreasing branch of hysteresis curve is obtained by tracing the magnetic field from H to $-H$. **The decreasing branch of the hysteresis curve is complete when the applied field reaches H value.** Similarly, using the spin configuration obtained after this process as initial configuration, the increasing branch of hysteresis curve is obtained by scanning the magnetic field from $-H$ to H . At each magnetic field step, the magnetization is collected over 5×10^4 Monte Carlo per step (MCSS) after the first 10^4 MCSS are discarded for equilibration process. The instantaneous magnetization components of the system can be calculated using the formula $M_\alpha = 1/N \sum_i S_{i\alpha}$. Here, N is the total number of the spins located on the hexagonal lattice, and $\alpha = x, y$ and z .

III. RESULTS AND DISCUSSION

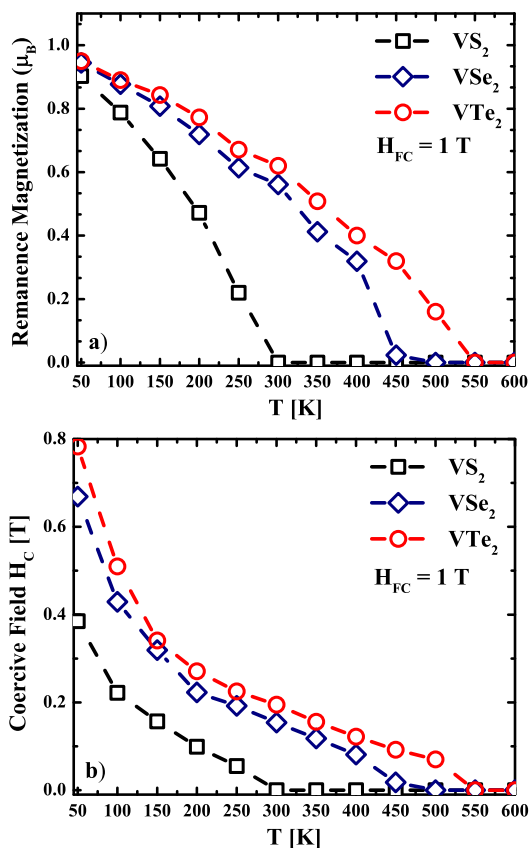


FIG. 1: (Color online) Variations of the (a) remanence magnetizations and (b) coercivities as functions of the temperature of the VX_2 monolayers. All curves are **calculated** under the field cooling $H_{FC} = 1T$ applied in parallel directions with respect to the VX_2 monolayers.

In Fig. 1, we give thermal dependencies of the remanence magnetizations and coercivities of the VX_2 monolayers. As shown in Fig. 1(a), remanence magnetization

treatments of the considered systems sensitively depend on the studied temperature value. In the lower temperature regions, VX_2 monolayers are in the strongly ferromagnetic phase. So, it is possible to observe bigger remanence values in this region. When the temperature is increased starting from relatively lower temperature, remanence magnetizations become to shift to the lower values. **This is a consequence of the fact** that increasing thermal energy tends to overcome the spin-spin interaction term between spin pairs and magnetic anisotropy energy in the system. As expected, if the temperature is increased further and is reached to a characteristic value, remanence magnetization tends to vanish. When one compares the obtained remanence magnetizations **as a function** of the temperature for VX_2 monolayers, one can easily see that **VTe₂ has much higher remanence value than the those found in other two materials.** As given in Fig. 1(b), **we also investigated the coercivity dependence on temperature for VX_2 monolayers.** It is possible to state that much more energy originating from external field is needed to reverse the sign of magnetization at the relatively lower temperature regions where VX_2 monolayers display strong ferromagnetic character. When the temperature is increased starting from lower temperature regions, coercive field values starts to decrease. Actually, this is an expected result since an increment in the temperature gives rise to the occurrence of more fluctuating behavior in the system, so coercive field gets narrower with increasing temperature value. These comments are also valid for all three monolayers studied here. If one compares the coercivity curves of VX_2 monolayers, one can see that **VTe₂ has a much higher coercivity value than those found in the other two materials.** It should be mentioned here that according to the Ref. [25], Curie temperatures of the (a) VS_2 , (b) VSe_2 and (c) VTe_2 monolayers are 292 K, 472 K and 553 K respectively. Our Monte Carlo results regarding the hysteresis features of VX_2 monolayers illustrate that it is possible to observe finite remanence and coercivity treatments nearly or well beyond room temperature. These findings also support **the previously reported** Curie temperatures mentioned above.

Final investigation has been devoted to determine the influences of the temperature on the hysteresis loops corresponding to remanence and coercivity features depicted in Fig. 1. In this regard, we represent hysteresis curves for (a) VS_2 , (b) VSe_2 and (c) VTe_2 monolayers for varying values of the temperature, as shown in Figs. 2(a-c). At first glance, shapes of the curves qualitatively resemble to each other. The hysteresis curves measured for all VX_2 monolayers clearly **reveal the ferromagnetism character.** In addition to these, **their shapes** explicitly depend on the studied temperature. For example, rectangular-shaped hysteresis curves obtained at the relatively lower temperature regions evolve into S-shape with increasing temperature. By comparing figures 2(a), (b) and (c) we observe that VSe_2 and VTe_2 monolayers evince ferromagnetism above room temperature.

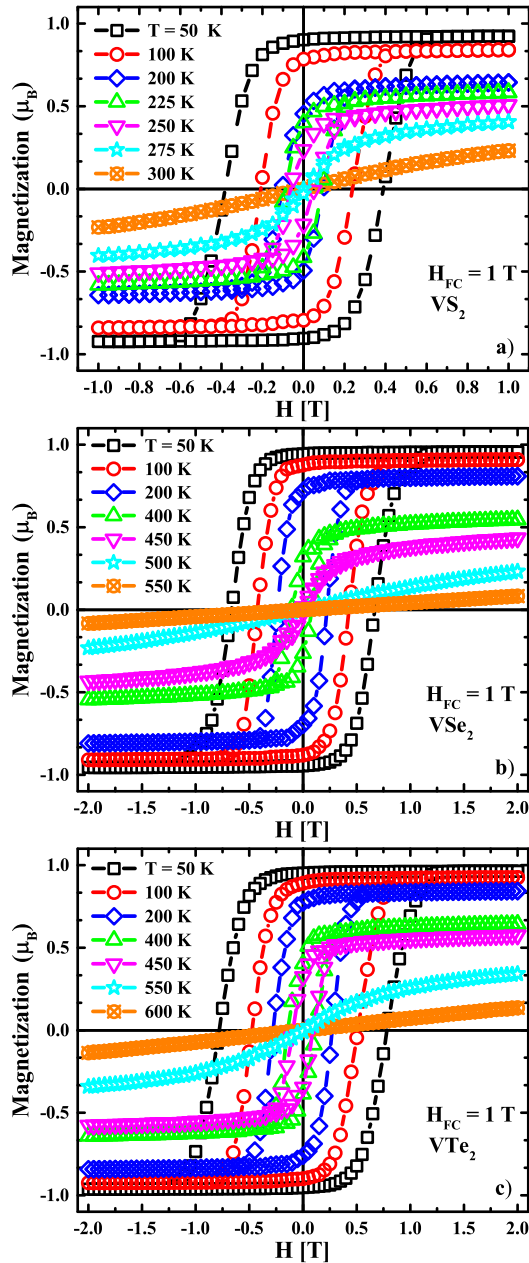


FIG. 2: (Color online) Effects of the temperature on the hysteresis curves of the (a) VS_2 , (b) VSe_2 and (c) VTe_2 monolayers. All curves are measured under the field cooling $H_{FC} = 1T$ applied in parallel directions with respect to the VX_2 monolayers.

In conclusion, we perform a detailed Monte-Carlo simulation based on the Metropolis algorithm to understand the hysteresis properties of the VX_2 monolayers. For this aim, we obtain hysteresis curves for a wide **range of temperature, up to 600 K**. All curves are measured under the field cooling $H_{FC} = 1T$ applied in parallel directions with respect to the VX_2 monolayers. **Results obtained** in this study suggest that both coercivity and remanence values **significantly** depend on the studied temperature. In other words, **both parameters** decrease prominently with increasing temperature. Moreover, it is found that hysteresis curves start to evolve from rectangular shaped observed at the lower temperature regions to nearly S-shaped as the temperature is further increased.

Acknowledgements

The numerical calculations reported in this paper were performed at TÜBİTAK ULAKBİM (Turkish agency), High Performance and Grid Computing Center (TRUBA Resources).

-
- [1] W.-Q. Han, L. Wu, Y. Zhu, K. Watanabe and T. Taniguchi, *Applied Physics Letters*, 2008, **93**, 223103
 - [2] P. Vogt, P. De Padova, C. Quaresima, J. Avila, E. Frantzeskakis, M. C. Asensio, A. Resta, B. Ealet and G. Le Lay, *Physical review letters*, 2012, **108**, 155501
 - [3] M. Dávila, L. Xian, S. Cahangirov, A. Rubio and G. Le Lay, *New Journal of Physics*, 2014, **16**, 095002
 - [4] S. Zhang, Z. Yan, Y. Li, Z. Chen and H. Zeng, *Angewandte Chemie*, 2015, **127**, 3155–3158
 - [5] H. Liu, A. T. Neal, Z. Zhu, Z. Luo, X. Xu, D. Tomnek and P. D. Ye, *ACS Nano*, 2014, **8**, 4033–4041
 - [6] K. Novoselov, D. Jiang, F. Schedin, T. Booth, V. Khotkevich, S. Morozov and A. Geim, *Proceedings of the National Academy of Sciences of the United States of America*, 2005, **102**, 10451–10453
 - [7] J. N. Coleman, M. Lotya, A. O'Neill, S. D. Bergin, P. J.

- King, U. Khan, K. Young, A. Gaucher, S. De, R. J. Smith *et al.*, *Science*, 2011, **331**, 568–571
- [8] M. Chhowalla, H. S. Shin, G. Eda, L.-J. Li, K. P. Loh and H. Zhang, *Nature chemistry*, 2013, **5**, 263–275
- [9] A. M. Appel, D. L. DuBois and M. Rakowski DuBois, *Journal of the American Chemical Society*, 2005, **127**, 12717–12726
- [10] H. I. Karunadasa, E. Montalvo, Y. Sun, M. Majda, J. R. Long and C. J. Chang, *Science*, 2012, **335**, 698–702
- [11] K. Chang and W. Chen, *ACS nano*, 2011, **5**, 4720–4728
- [12] B. Radisavljevic, A. Radenovic, J. Brivio, i. V. Giacometti and A. Kis, *Nature nanotechnology*, 2011, **6**, 147–150
- [13] Q. H. Wang, K. Kalantar-Zadeh, A. Kis, J. N. Coleman and M. S. Strano, *Nature nanotechnology*, 2012, **7**, 699–712
- [14] G. R. Bhimanapati, Z. Lin, V. Meunier, Y. Jung, J. Cha, S. Das, D. Xiao, Y. Son, M. S. Strano, V. R. Cooper, L. Liang, S. G. Louie, E. Ringe, W. Zhou, S. S. Kim, R. R. Naik, B. G. Sumpter, H. Terrones, F. Xia, Y. Wang, J. Zhu, D. Akinwande, N. Alem, J. A. Schuller, R. E. Schaak, M. Terrones and J. A. Robinson, *ACS Nano*, 2015, **9**, 11509–11539
- [15] R. Shidpour and M. Manteghian, *Nanoscale*, 2010, **2**, 1429–1435
- [16] J. He, K. Wu, R. Sa, Q. Li and Y. Wei, *Applied Physics Letters*, 2010, **96**, 082504
- [17] Z. Wang, K. Zhao, H. Li, Z. Liu, Z. Shi, J. Lu, K. Suenaga, S.-K. Joung, T. Okazaki, Z. Jin *et al.*, *Journal of Materials Chemistry*, 2011, **21**, 171–180
- [18] Y. Li, Z. Zhou, S. Zhang and Z. Chen, *Journal of the American Chemical Society*, 2008, **130**, 16739–16744
- [19] Y. Ma, Y. Dai, M. Guo, C. Niu and B. Huang, *Nanoscale*, 2011, **3**, 3883–3887
- [20] Y. Ma, Y. Dai, M. Guo, C. Niu, J. Lu and B. Huang, *Physical Chemistry Chemical Physics*, 2011, **13**, 15546–15553
- [21] Y. Ma, Y. Dai, M. Guo, C. Niu, Y. Zhu and B. Huang, *ACS Nano*, 2012, **6**, 1695–1701
- [22] Y. Zhou, Z. Wang, P. Yang, X. Zu, L. Yang, X. Sun and F. Gao, *Acs Nano*, 2012, **6**, 9727–9736
- [23] M. Kan, B. Wang, Y. H. Lee and Q. Sun, *Nano Research*, 2015, **8**, 1348–1356
- [24] D. Gao, Q. Xue, X. Mao, W. Wang, Q. Xu and D. Xue, *Journal of Materials Chemistry C*, 2013, **1**, 5909–5916
- [25] H.-R. Fuh, C.-R. Chang, Y.-K. Wang, R. F. Evans, R. W. Chantrell and H.-T. Jeng, *Scientific Reports*, 2016, **6**, 32625
- [26] D. W. Murphy, C. Cros, F. Di Salvo and J. Waszczak, *Inorganic Chemistry*, 1977, **16**, 3027–3031
- [27] J. Feng, X. Sun, C. Wu, L. Peng, C. Lin, S. Hu, J. Yang and Y. Xie, *Journal of the American Chemical Society*, 2011, **133**, 17832–17838
- [28] J. Feng, L. Peng, C. Wu, X. Sun, S. Hu, C. Lin, J. Dai, J. Yang and Y. Xie, *Advanced materials*, 2012, **24**, 1969–1974
- [29] H. Zhang, L.-M. Liu and W.-M. Lau, *Journal of Materials Chemistry A*, 2013, **1**, 10821–10828
- [30] C. S. Rout, B.-H. Kim, X. Xu, J. Yang, H. Y. Jeong, D. Odkhuu, N. Park, J. Cho and H. S. Shin, *Journal of the American Chemical Society*, 2013, **135**, 8720–8725
- [31] C. Song, K. Yu, H. Yin, H. Fu, Z. Zhang, N. Zhang and Z. Zhu, *Journal of Materials Chemistry C*, 2014, **2**, 4196–4202
- [32] N. D. Boscher, C. S. Blackman, C. J. Carmalt, I. P. Parkin and A. G. Prieto, *Applied surface science*, 2007, **253**, 6041–6046
- [33] R. Guzmán, P. Lavela, J. Morales, J. Tirado *et al.*, *Journal of applied electrochemistry*, 1997, **27**, 1207–1211
- [34] A. Thompson, J. Scanlon and C. Symon, *Solid State Ionics*, 1980, **1**, 47–57
- [35] A. Vinokurov, A. Tyurin, A. Emelina, K. Gavrichiev and V. Zlomanov, *Inorganic Materials*, 2009, **45**, 480–485
- [36] Y. Zhang and X. Wu, *Physics Letters A*, 2013, **377**, 3154–3157
- [37] L.-Y. Gan, Q. Zhang, Y. Cheng and U. Schwingenschlög, *Physical Review B*, 2013, **88**, 235310
- [38] H. Pan, *Scientific Reports*, 2014, **4**, year
- [39] M. Zhong, Y. Li, Q. Xia, X. Meng, F. Wu and J. Li, *Materials Letters*, 2014, **124**, 282–285
- [40] H. Pan, *The Journal of Physical Chemistry C*, 2014, **118**, 13248–13253
- [41] A. H. M. A. Wasey, S. Chakrabarty and G. P. Das, *Journal of Applied Physics*, 2015, **117**, 064313
- [42] Y. Qu, H. Pan, C. T. Kwok and Z. Wang, *Nanoscale research letters*, 2015, **10**, 480
- [43] P.-R. Huang, Y. He, H. K. Pal and M. Kindermann, *arXiv preprint arXiv:1501.00760*, 2015
- [44] H. L. Zhuang and R. G. Hennig, *Physical Review B*, 2016, **93**, 054429
- [45] T. Wang, Y. Li, C. Xia, X. Zhao, Y. An and X. Dai, *Journal of Materials Chemistry C*, 2016, **4**, 8111–8120
- [46] N. Luo, C. Si and W. Duan, *Physical Review B*, 2017, **95**, 205432
- [47] D. Gao, J. Li, Z. Li, Z. Zhang, J. Zhang, H. Shi and D. Xue, *The Journal of Physical Chemistry C*, 2010, **114**, 11703–11707
- [48] C. Wang, Q. Wu, H. Ge, T. Shang and J. Jiang, *Nanotechnology*, 2012, **23**, 075704
- [49] C. Ataca, H. Sahin and S. Ciraci, *The Journal of Physical Chemistry C*, 2012, **116**, 8983–8999
- [50] K. Binder, *Monte Carlo Methods in Statistical Physics*, Springer-Verlag Berlin Heidelberg, 1979
- [51] M. E. J. Newman and G. T. Barkema, *Monte Carlo Methods in Statistical Physics*, Oxford University Press: New York, USA, 1999